

The relative roles of tropical and extratropical forcing on atmospheric variability

Andreas Sterl and Wilco Hazeleger

Royal Netherlands Meteorological Institute (KNMI), De Bilt, Netherlands

Received 8 June 2005; revised 1 August 2005; accepted 22 August 2005; published 29 September 2005.

[1] A fast atmospheric General Circulation Model is used to generate three ensembles of atmospheric circulation. While the first ensemble is forced by global sea surface temperature (SST) anomalies, the forcing is confined to the tropics and extratropics, respectively, in the other two ensembles. The tropical SST anomalies have the largest impact on atmospheric variability. However, also the extratropical SST has a systematic effect on the atmosphere. In the Southern Hemisphere the extratropically forced signal reaches the strength of the tropically forced one on decadal time scales. The atmospheric response to global SST anomalies can be understood as a nearly linear superposition of the reactions to tropical and extratropical forcing, respectively, or, in a different view, as a superposition of a thermodynamic response to the global-mean SST anomaly and a dynamic response to local SST anomalies, the most important being El Niño. **Citation:** Sterl, A., and W. Hazeleger (2005), The relative roles of tropical and extratropical forcing on atmospheric variability, *Geophys. Res. Lett.*, 32, L18716, doi:10.1029/2005GL023757.

1. Introduction

[2] According to a review article by *Kushnir et al.* [2002] the question central to the debate on the role of the ocean in extratropical climate variability “is whether the influence of the extratropical ocean extends beyond the local thermodynamic response of the marine boundary layer to affect the evolution and dynamical properties of the large-scale atmospheric circulation.” Their answer is that there is indeed an influence that goes beyond the marine boundary layer, but that its amplitude is small compared to the internal variability of the atmosphere. This paper tries to quantify that amplitude and investigates the relative roles of tropical and extratropical forcing, respectively. To this end we force a fast atmospheric General Circulation Model (AGCM) with 123 years of observed/reconstructed SST data. The forced atmospheric response is separated from the internal noise by performing ensembles of runs and investigating the ensemble-mean.

[3] The experimental set-up is similar to that of *Lau and Nath* [1994] who use ensembles with geographically confined SST forcing to identify the importance of different regions in forcing the atmosphere. *Rowell* [1998] uses a statistical method (ANOVA) to identify

regions of potential predictability. Several recent papers dealt with trends and their origin in the atmospheric circulation of the Northern Hemisphere (NH) during the second half of the last century [e.g., *Bracco et al.*, 2004; *Hurrell et al.*, 2004; *Schneider et al.*, 2003]. Major differences between the present study and those mentioned above are the consideration of both hemispheres and a much longer period of time.

2. Model Runs and Data Preparation

[4] The experiments in this paper are conducted with SPEEDY, a primitive equation atmosphere model with simplified physics parameterization [*Molteni*, 2003]. The version used here has seven vertical levels and a horizontal resolution of T30 [*Hazeleger et al.*, 2003].

[5] The SPEEDY runs are forced by SST anomalies derived from ERSST [*Smith and Reynolds*, 2003], spanning the period 1880 to 2002. In order to separate a small signal from the large atmospheric noise (“internal variability”) ensemble integrations using identical forcing are performed. The ensemble-mean then contains the forced response (“signal”) as the noise is averaged out. Unless otherwise stated all results presented in this paper are for ensemble-means. The ensemble members only differ in the initial condition of the AGCM. The ensembles differ in the spatial extent of the SST anomalies: global (GL), only tropics (TR), and only extratropics (ET). The boundary between tropics and extratropics is chosen to be at 20° on either side of the equator, and the anomalies are smoothly reduced to zero across the boundaries.

[6] GL and ET both contain 20 members, while TR is made up of only 10 members. To assess the robustness of the results GL and ET are divided into two 10-member sub-ensembles. For GL the main variability patterns from the two sub-ensembles are nearly identical. For ET they differ in detail, but agree on the large scale. From this we conclude that 10 members are enough for an ensemble including tropical forcing, while 20 is more appropriate for the extratropically forced one.

[7] Throughout the paper monthly-mean data are used. Monthly-mean anomalies are calculated by subtracting from each individual monthly mean the long-term mean of the corresponding calendar month. The data are smoothed by a 12 month running-mean (12mrm) filter to remove high-frequency variability. The filtering hardly changes the main variability patterns nor their low-frequency variations, but increases the fraction of variance they explain.

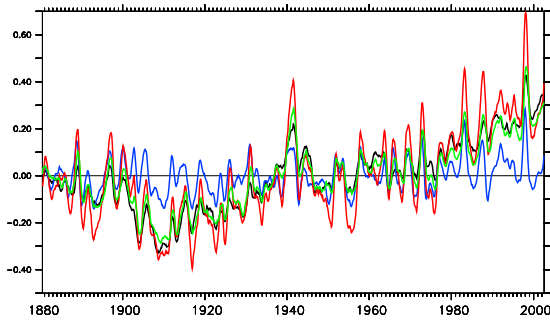


Figure 1. Anomalies from GL. Black, global-mean SST (K); blue, SST in the NINO3 region (150°W – 90°W , 5°S – 5°N)(10 K); red, SST in the tropical belt (20°S – 20°N)(K); and green, global-mean 500 hPa height (30 m).

[8] We do not remove a linear trend from the data prior to analysis as Figure 1 shows that the trend differs widely between different sub-periods.

3. Globally Forced Runs

3.1. Global-Mean Response

[9] The prescribed SST forcing contains two global trends. During the first ≈ 40 years global-mean SST decreased, while it increased during most of the remaining time (Figure 1, black). Superimposed on these two trends is some short-term variability which is due to ENSO (El Niño-Southern Oscillation) as can be seen from the blue curve. The red line in Figure 1 gives the SST anomaly averaged over the tropical belt. Obviously, tropical and global SST variations are nearly identical. Extratropically averaged SST exhibits the same long-term variations as tropically averaged SST, but lacks the El Niño-type short-term fluctuations (not shown).

[10] When the globally averaged SST varies, the globally-averaged temperature of the lower atmosphere varies accordingly. A higher (lower) temperature of the atmosphere will lift (lower) the centre-of-mass of the atmosphere, with a corresponding lifting (lowering) of the 500 hPa height level (Figure 1, green). This response is purely thermodynamic. The globally-averaged anomalies of 500 hPa height (Δz_{500}) and surface atmospheric temperature (ΔST) are found to be related by

$$\frac{\Delta z_{500}}{\Delta ST} \approx 20 \text{ m/K.} \quad (1)$$

This relation compares well with linear theory [Kushnir *et al.*, 2002, equation (3.1)] and holds down to interannual time scales. It is also valid for individual runs and all ensembles. By construction, the sum of the SST anomalies from TR and ET equals that from GL, and the same turns out to be true for z_{500} (not shown). Thus the global-mean atmospheric response seems to be partly extratropically driven. Note that this does not imply predictability as the extratropical SST itself is a result of chaotic atmospheric forcing (see the discussion by Kushnir *et al.* [2002]).

3.2. Variability Patterns

[11] The main modes of atmospheric variability and their forcing SST patterns are found by calculating Empirical Orthogonal Functions (EOF) of the ensemble-mean data of GL. The first two EOF patterns of 500 hPa height and surface temperature (ST) and their Principle Components (PC) are shown in Figure 2. We use ST rather than SST to incorporate the induced temperature signal over land. For both EOFs the PCs of ST and z_{500} are highly correlated, confirming that they describe the same mode of variability. The first two EOFs are well separated from the third which only explain 6.5% (ST) and 5.8% (z_{500}) of the variance.

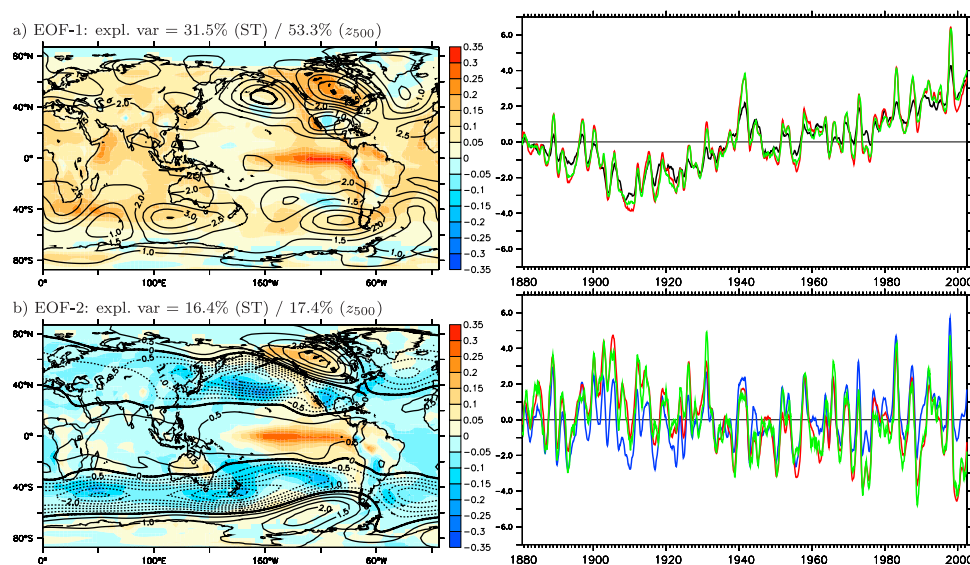


Figure 2. (left) First two EOFs of surface temperature (ST, in colour) and z_{500} (isolines, contour interval = 0.5 m, zero line thick) from GL. (right) The corresponding PCs (red, ST; green, z_{500}). Superimposed in black and blue are, respectively, the global-mean SST (scaled by 10) and NINO3 index (scaled by 2). These curves correspond to those of the same colour in Figure 1.

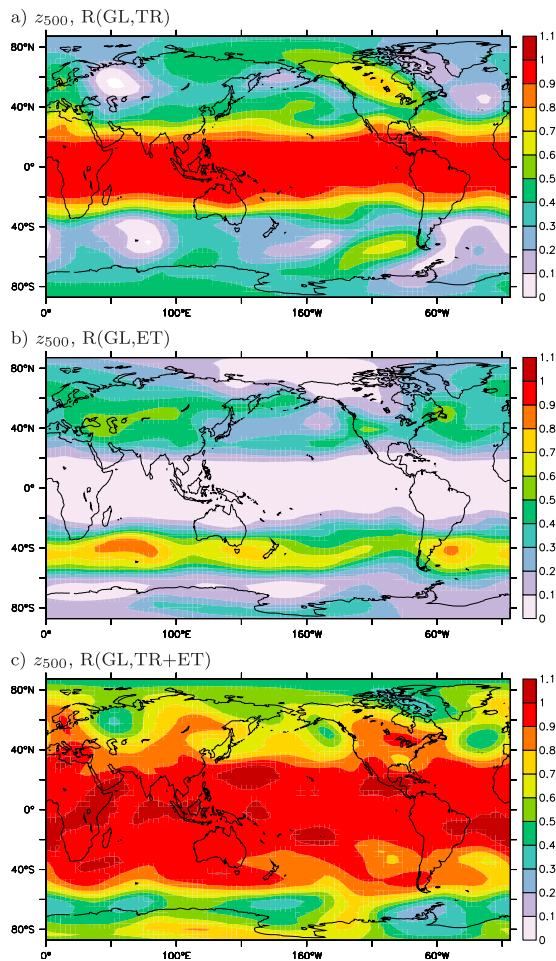


Figure 3. Regression coefficient R between 500 hPa height anomalies in GL and (a) TR and (b) ET, and (c) the sum of TR and ET.

[12] The PCs of the first EOFs are highly correlated with the globally-averaged SST (black line in Figure 2a), identifying this pattern as the thermodynamic response of the atmosphere to global SST changes. The signal has the same sign nearly everywhere. The temperature signal contains the signature of ENSO (correlation of -0.7 with the NINO3 index), and the 500 hPa height signal is nearly globally homogeneous and only modulated between 40° and 60° in both hemispheres. The modulation is largest over the North Pacific/North America (NPA) region. This ENSO-like pattern (see below) is forced by the ENSO-like SST-pattern in the ST EOF.

[13] The second EOF represents that part of the ENSO signal that does not project onto the global signal. The PCs are highly correlated with the NINO3 index (blue line in Figure 2b). For ST it has the largest amplitude over the Pacific basin, where high values along the equator are flanked by high values of the opposite sign to the northwest and southwest. The corresponding atmospheric response (z_{500}) is nearly symmetric around the equator. It shows the typical ENSO response, consisting of hemispherically symmetric wave trains emanating from the SST anomaly [Trenberth *et al.*, 1998; Seager *et al.*, 2003]. While EOF-1

describes the thermodynamic response of the atmosphere, EOF-2 represents the most important dynamical response.

4. Regionally Forced Runs

[14] Although not identical, the first two EOFs of z_{500} from both GL and TR (not shown) describe the same modes of variability, consisting mainly of a trend, a strong signal in the NPA region and a nearly zonal symmetric signal south of 40° S. On the contrary, the ET EOFs (not shown) are all nearly zonally symmetric. The first of them shows some modulation in the Southern Hemisphere (SH) matching that in the second EOF from GL, and the two PCs are correlated at 0.53. A closer inspection shows that along 40° S the first EOF of ET explains more variance of GL than the first two EOFs of TR together. Thus part of the forced variability in 500 hPa height in this area results from extratropical SST.

[15] To further investigate the relative importance of respectively tropical and extratropical forcing in generating atmospheric variability, Figure 3 shows maps of the pointwise regression coefficients R of z_{500} between GL and respectively TR, ET and TR + ET. We use regression rather than correlation as the former also contains information on the amplitude of the signals. For $R = 1$ the two signals are identical. Values close to 1 are found in the tropics for the comparison between GL and TR (Figure 3a), confirming that tropical atmospheric variability is driven by tropical SST. In four other areas variability is also forced to a certain extent by tropical SST: the central North Pacific and large parts of North America in the NH and their mirror-images in the SH. These are the same areas that show up in the second EOF of z_{500} (Figure 3b). Note that contrary to the results of Lau and Nath [1994] the signal is larger over North America than over the North Pacific.

[16] The extratropical SST is much less effective in producing a forced atmospheric signal (Figure 3b). The magnitude of R is generally low and exceeds 0.6 only in a zonal strip along 40° in the SH, well outside the region of large R -values in TR. This suggests that tropically and extratropically forced variabilities, respectively, are independent. Indeed, the sum of TR and ET (Figure 3c) gives a better representation of the full signal (GL) than either of them alone.

[17] The impact of extratropical SST on atmospheric circulation in the SH solely results from the long time scale: After subtracting that part of the variability that is linearly related to the global-mean SST (the regression of z_{500} on global-mean SST) and repeating the analysis leading to Figure 3c no common signal is left along 40° S. If, on the other hand, we filter the data with a 60mm the regression between GL and ET in the SH becomes much stronger.

5. Internal Variability

[18] The foregoing analysis showed that there is a systematic influence of the extratropical SST on the atmospheric circulation. However, the variability in each ensemble member is a combination of forced and internal variability. To obtain the internal variability, we subtract the ensemble mean, i.e., the forced signal, from each individual ensemble member. The resulting fields are concatenated, and the concatenated field is analyzed.

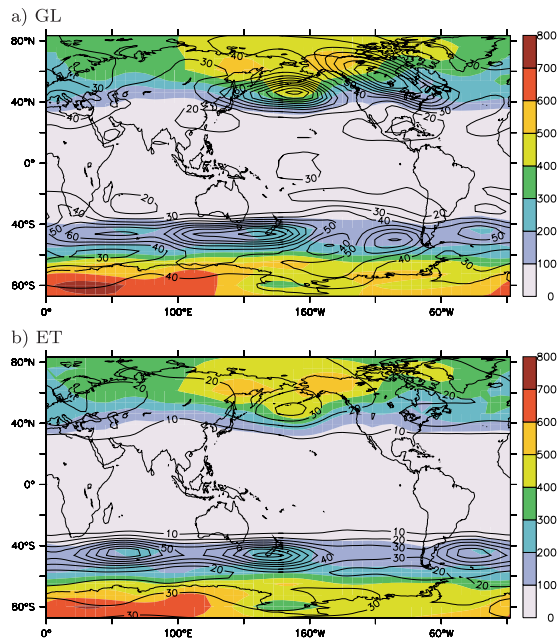


Figure 4. Internal (color) and forced (isolines) variance of z_{500} in ensembles (a) GL and (b) ET.

[19] Figure 4 compares the temporal variances of the forced and the internal variabilities, respectively. The first is calculated from the anomalies of the ensemble mean, the second from the concatenated anomalies just described. The similarity of the internally generated variances (colours) in ensembles GL and ET indicates that the separation into internally generated and externally forced variability was successful. In GL the strength of the forced signal is about 25% of the internal noise in the NH and about 50% between 40°S and 60°S. In ET the forced signal in the NH is a factor 4–5 lower than it is in GL (i.e., only about 5% of the internal noise), but it is of equal strength south of $\approx 40^\circ\text{S}$. The result for the NH confirms the conclusion of Kushnir *et al.* [2002], while that for the SH backs our earlier finding of a discernable, extratropically forced signal in this region. The same analysis for TR (not shown) confirms these findings: the internal variability is similar to that in GL and ET, while the forced signal is much lower than in GL south of 40°S, but only slightly lower in the NPA region.

[20] Repeating the analysis for respectively unfiltered and heavily-smoothed (60mm) data confirms this result. While there is no difference between the hemispheres for the unfiltered data with forced variability below 10% of the internal noise, the forced signal exceeds internal variability for 60mm-filtered data by up to a factor of two in the SH.

6. Summary and Conclusion

[21] Using the fast atmospheric model SPEEDY [Molteni, 2003] we have performed three ensembles of runs forced by observed SSTs between 1880 and 2002. The ensembles differ in the spatial extent of the prescribed SST

anomalies: global, tropics, and extratropics. The purpose of these experiments was to identify SST-forced patterns of atmospheric variability and determine their geographic origin.

[22] The forced atmospheric variability can be decomposed into a thermodynamic mode characterized by a nearly homogenous lifting/lowering of the whole atmosphere as a response to changes in the global-mean surface temperature, and a dynamic mode consisting of a wave-like pattern that is centered around the El Niño region and nearly symmetric between the two hemispheres. While this mode is clearly of tropical origin, the first one also contains an extratropical component. The sum of the two partially forced runs better represents the variability of the globally forced run than either of them alone. Thus extratropical SST has a systematic impact on the atmospheric circulation that goes beyond the marine boundary layer. This impact is much larger in the SH than it is in the NH and only discernible for decadal time scales.

[23] **Acknowledgments.** Data analysis and plotting was done with the free Ferret software developed at NOAA/PMEL (see <http://www.ferret.noaa.gov>). We thank Camiel Severijns for his invaluable software support. The comments of an anonymous reviewer greatly improved the paper.

References

- Bracco, A., F. Kucharski, R. Kallummal, and F. Molteni (2004), Internal variability, external forcing and climate trends in multi-decadal AGCM ensembles, *Clim. Dyn.*, *23*, 659–678, doi:10.1007/s00382-004-0465-2.
- Hazeleger, W., C. Severijns, R. Haarsma, F. Selten, and A. Sterl (2003), SPEEDO—Model description and validation of a flexible coupled model for climate studies, *Techn. Rep. TR-257*, R. Neth. Meteorol. Inst. (KNMI), De Bilt, Netherlands.
- Hurrell, J. W., M. P. Hoerling, A. Phillips, and T. Xu (2004), Twentieth century North Atlantic climate change: Part I. Assessing determinism, *Clim. Dyn.*, *23*, 371–389, doi:10.1007/s00382-004-0432-y.
- Kushnir, Y., W. A. Robinson, I. Bladé, N. M. J. Hall, S. Peng, and R. Sutton (2002), Atmospheric GCM response to extratropical SST anomalies: Synthesis and evaluation, *J. Clim.*, *15*, 2233–2256.
- Lau, N.-C., and M. J. Nath (1994), A modelling study of the relative roles of tropical and extratropical SST anomalies in the variability of the global atmosphere-ocean system, *J. Clim.*, *7*, 1184–1207.
- Molteni, F. (2003), Atmospheric simulations using a GCM with simplified physical parameterizations: I. Model climatologies and variability in multi-decadal experiments, *Clim. Dyn.*, *20*, 175–191, doi:10.1007/s00382-002-0268-2.
- Rowell, D. P. (1998), Assessing potential seasonal predictability with an ensemble of multidecadal GCM simulations, *J. Clim.*, *11*, 109–120.
- Schneider, E. K., L. Bengtsson, and Z.-Z. Hu (2003), Forcing of Northern Hemisphere climate trends, *J. Atmos. Sci.*, *60*, 1504–1521.
- Seager, R., N. Harink, Y. Kushnir, W. Robertson, and J. Miller (2003), Mechanisms of hemispherically symmetric climate variability, *J. Clim.*, *16*, 2960–2978.
- Smith, T. M., and R. W. Reynolds (2003), Extended reconstruction of global Sea Surface Temperatures based on COADS data (1854–1997), *J. Clim.*, *16*, 1495–1510.
- Trenberth, K. E., G. W. Branstator, D. Karoly, A. Kumar, N.-C. Lau, and C. Ropelewski (1998), Progress during TOGA in understanding and modeling global teleconnections associated with tropical sea surface temperatures, *J. Geophys. Res.*, *103*, 14,291–14,324.

W. Hazeleger and A. Sterl, Royal Netherlands Institute of Meteorology (KNMI), P.O. Box 201, NL-3730 AE De Bilt, Netherlands. (hazelege@knmi.nl; sterl@knmi.nl)